



Article

Preform Porosity and Final Thickness Variability Prediction after Controlled Post-Infusion External Pressure Application with the FEA Model

Igor Zhilyaev ¹, Shun-Hsyung Chang ², Sergey Shevtsov ^{3,*}  and Natalia Snezhina ⁴

¹ Institute of Polymer Engineering, The University of Applied Sciences Northwestern Switzerland FHNW, CH-5210 Windisch, Switzerland

² Department of Microelectronics Engineering, National Kaohsiung University of Science and Technology, Kaohsiung City 82445, Taiwan

³ Department of Transport, Composite Materials and Structures, Southern Center of Russian Academy of Science, 344006 Rostov on Don, Russia

⁴ Department of Aircraft Engineering, Don State Technical University, 344000 Rostov on Don, Russia

* Correspondence: sergnshevtsov@gmail.com

Abstract: One of the reasons for the insufficiently wide use of the low-cost and low-labor vacuum infusion process in the production of polymer composite structures is the uneven distribution of pore pressure, porosity, and preform thickness at the final stage of filling the preform with liquid resin. This article presents the results of a theoretical study of the factors that govern the effectiveness of the known method of external controlled pressure on the preform in order to eliminate or significantly reduce the listed disadvantages. The study includes an analysis of scenarios for the implementation of this method, which differ in the state of the resin gate when external pressure is applied to the preform (open or closed), as well as the pressure in the vacuum vent (maintained unchanged or gradually increased to atmospheric pressure). The research tool was a finite element (FE) model that simulates resin flow according to Darcy's law and controlled boundary conditions for a thin-walled rectangular preform. The results of the study confirmed the effectiveness of the process in achieving a more uniform distribution of porosity and preform thickness and are in good qualitative agreement with the results of borrowed experiments, revealing the conditions for the occurrence of critical situations associated with the possible penetration of air into the preforms through the vacuum port and the reverse flow into the preform of the resin previously forced out through the resin gate.

Keywords: polymeric composite technology; vacuum infusion; preform porosity and wall thickness uniformity; post-infusion external pressure application; finite-element modeling; controlled process variables; optimum design of the process mode



Citation: Zhilyaev, I.; Chang, S.-H.; Shevtsov, S.; Snezhina, N. Preform Porosity and Final Thickness Variability Prediction after Controlled Post-Infusion External Pressure Application with the FEA Model. *J. Compos. Sci.* **2022**, *6*, 361. <https://doi.org/10.3390/jcs6120361>

Academic Editor: Francesco Tornabene

Received: 1 October 2022

Accepted: 23 November 2022

Published: 25 November 2022

Publisher's Note: MDPI stays neutral with regard to jurisdictional claims in published maps and institutional affiliations.



Copyright: © 2022 by the authors. Licensee MDPI, Basel, Switzerland. This article is an open access article distributed under the terms and conditions of the Creative Commons Attribution (CC BY) license (<https://creativecommons.org/licenses/by/4.0/>).

1. Introduction

In the last two decades, vacuum-assisted technologies for the manufacturing of polymeric composite structures have become increasingly in demand in aerospace engineering, the production of wind turbines, shipbuilding, and civil engineering [1–3]. A common component of the kind of such technologies (VARTM, SCRIMP, RFI et al.) is the injection of liquid resin into a dry porous preform and its propagation therein under the action of a pressure gradient [4]. Such technologies usually include three successive stages: preparation and laying-up of preform layers, covered with a flexible vacuum bag and carefully isolated from atmospheric air; filling the preform with liquid resin injected from the resin gate and moving towards the vacuum vent; and the final stage, which may include additional exposure of the filled preform to increased temperature and pressure [2]. The fulfillment of the most important requirements for mechanical and strength properties, geometric accuracy, and climatic resistance of the molded part are determined by the values of the fiber volume fraction and the uniformity of its distribution in the preform, the void volume,

provided at each of the three stages of the manufacturing process [5–8]. The research results presented in these papers show that the properties of parts manufactured using the infusion technology, usually are inferior to those manufactured using the hot-pressing technology of pre-impregnated prepregs, especially in terms of ensuring the permissible voids volume, as well as the required values of the fiber volume fraction and the uniformity of its spatial distribution across the preform. The preform is a compressible poroelastic frame, the sections of which are completely or partially filled with resin with varying pressure. Its increase leads to the expansion of pores, a decrease in the relative volume of reinforcement, and an increase in the thickness of the preform [9–19]. Thus, a gain in the pore pressure gradient leads to an increase in the resin velocity and, consequently, the performance of the vacuum infusion process, which contradicts the requirement to ensure uniform distribution of the fiber volume fraction and preform thickness. In addition, the poor repeatability of the process, due to its high sensitivity to the layout and regimes, has become an obstacle to its widespread use in high-tech industries.

Numerous studies have been aimed at finding reliable methods for monitoring the state of the preform during its filling with liquid resin. Among them are such sophisticated ones as a monitoring the 3D resin flow using hybrid piezoelectric-fiber sensor network or optical frequency domain reflectometry and long-gauge FBG sensors [20,21]. As technological improvements to overcome the noted difficulties, the post-infusion exposure during vacuum infusion of thermosetting composites reinforced with thermoplastic interlayer veils [22] and fiber prestressing to prevent their fraying and weakening during infusion [23,24] have been proposed. In addition, an effective and apparently very general solution could be the technology of controlled post-infusion external pressure, the various strategies of which have received a reliable experimental justification in [25,26]. The proposed method requires some complication of technological equipment but can be implemented without significant costs in the practice of manufacturing a wide range of polymer-composite structures. In the cited works, studies were carried out with samples of preforms of the simplest shape and relatively small sizes. Obviously, in order to obtain the necessary information about the phenomena that occur during the implementation of the process on larger more complex parts, it is necessary to understand how the size, shape of the parts, properties of resins and porous preforms will affect its results. In the presented article, this problem is investigated theoretically using a specially developed simulation tool. In one of the first works considering the post-infusion stage of the process [27], a one-dimensional model based on a compressed sponge is presented, which allows to predict the compaction of a thick-walled laminate. In most models [12,18,28,29], considerable attention is paid to the correct description of the compressive properties of porous preforms in both dry and wet states, providing the condition of conservation the resin mass flow.

Due to the fact that the state of a compressible preform filled with liquid resin can be estimated in the experiment only by normal displacements of points on its open surface, relations were developed in [10,30] that couple the magnitude of these displacements with local changes in strains, porosity and fiber volume fraction. The experimental methods used for this purpose and confirmation of their reliability are described in detail in [25,26,31,32]. The presented study is focused on the development of software tools designed to simulate the post-infusion impact on the preform by controlled external pressure according to the methodology described in [13,15,25,26], where it is always assumed that the preform is initially completely filled with liquid resin. In practice, this requirement is not always met due to incomplete impregnation of the entire volume with resin and the formation of dry spots in different parts of the infused preform. That is why the software module described below was developed as a compatible addition to the software tool described in [33,34] and capable of simulating the actual infusion stage. The modeling method used in the described module is based on poroelasticity relations; and its operation as a stand-alone for clarity and better understanding is illustrated by a simplified example of a rectangular preform. It is assumed that in the initial state, the preform is completely filled with liquid resin, the pressure and viscosity of which are subject to certain distributions,

adopted according to some reasonable assumptions. Thermal and thermo-kinetic effects are excluded from consideration.

The text of the article is structured as follows. Initially, the relations of classical poroelasticity and the flow of a viscous fluid in a porous medium are considered with their adaptation to the case of a thin-walled preform with a fixed lower surface. It is assumed that the preform has a transversal isotropy of elastic properties and permeability. The resulting model description of preform deformations, associated changes in porosity and permeability, which affect the flow of viscous resin, obtained as a result of these assumptions, is used in the finite element formulation of the problem. Next, two scenarios for the implementation of the post-infusion stage of the process are considered, which begin after the stabilization of the resin flow, when the inlet (through the resin gate) and outlet (through the vacuum valve) flows are equalized. At this moment, a gradual increase in pressure begins, which acts on the open outer surface of the preform, which can be accompanied by a controlled rise of the outlet pressure to atmospheric pressure with a varying delay. In the first scenario, both the inlet and outlet are open throughout the entire process, while in the second, the resin gate is closed from the start of the applied external pressure. The following analysis of the simulation results allows to identify the composition and influence of the controlled factors of the process on its final results, as well as to find situations that can lead to the irreparable defects in the molded composite part.

2. Modeling Problem Statement

An analysis of the scenarios for application of controlled external pressure on a composite preform, studied experimentally in [25,26], demonstrates their similarity to the situation considered in the classical Mandel’s problem [35], when a compressive external force acts on a certain porous volume filled with liquid. This volume has part of the open boundaries and part of the closed, preventing the outflow of fluid outward. The full set of the constitutive equations consists of the displacements \mathbf{u} in poroelastic body, the equation for the internal pressure, the equilibrium equation, the Darcy’s law and the continuity equation for the fluid content. These equations can be transformed to the system of Navier–Cauchy, which in the case of a transversely isotropic (xy plane of transversal isotropy) porous material has the form (1), and diffusion Equation (2) for the pore pressure p_m [31].

$$\begin{aligned}
 M_{xx} \frac{\partial^2 u_x}{\partial x^2} + G \frac{\partial^2 u_x}{\partial y^2} + G' \frac{\partial^2 u_x}{\partial z^2} + (M_{xy} + G) \frac{\partial^2 u_y}{\partial x \partial y} + (M_{xz} + G') \frac{\partial^2 u_z}{\partial x \partial z} - \alpha_x \frac{\partial p_m}{\partial x} &= 0 \\
 G \frac{\partial^2 u_y}{\partial x^2} + M_{xx} \frac{\partial^2 u_y}{\partial y^2} + G' \frac{\partial^2 u_y}{\partial z^2} + (M_{xy} + G) \frac{\partial^2 u_x}{\partial x \partial y} + (M_{xz} + G') \frac{\partial^2 u_z}{\partial y \partial z} - \alpha_x \frac{\partial p_m}{\partial y} &= 0 \\
 G' \frac{\partial^2 u_z}{\partial x^2} + G' \frac{\partial^2 u_z}{\partial y^2} + M_{zz} \frac{\partial^2 u_z}{\partial z^2} + (M_{xz} + G') \frac{\partial^2 u_x}{\partial x \partial z} + (M_{xz} + G') \frac{\partial^2 u_y}{\partial y \partial z} - \alpha_z \frac{\partial p_m}{\partial z} &= 0
 \end{aligned} \tag{1}$$

$$\frac{\partial p_m}{\partial t} - \kappa_x M \frac{\partial^2 p_m}{\partial x^2} - \kappa_x M \frac{\partial^2 p_m}{\partial y^2} - \kappa_z M \frac{\partial^2 p_m}{\partial z^2} = -\alpha_x M \left(\frac{\partial e_{xx}}{\partial t} + \frac{\partial e_{yy}}{\partial t} \right) - \alpha_z M \frac{\partial e_{zz}}{\partial t} \tag{2}$$

In these equations $M_{xx}, M_{xy}, M_{xz}, M_{zz}$ are the components of the stiffness matrix, expressed in terms of Young’s moduli and Poisson’s ratios of the material, G and G' are the shear moduli in the xy and xz (yz) planes, respectively [35]. The source term in Equation (2) contains the time derivatives of the strain e_{ij} in a porous medium, which can be expressed through the solution of Equation (1).

All relations given below were obtained under the following assumptions. The preform of a molded composite structure is a thin-walled body, which lower surface is fixed. The external pressure p_{appl} applied to the upper preform surface and the pore pressure p_m cause only changes in the thickness of the preform, whose compressibility dependence on the strain is the same at every point in the preform. The material of the porous frame is

considered homogeneous, the microstructure of which is neglected. So, taking into account these assumptions, the Biot modulus M can be expressed as [35]

$$M = \left[\phi / K_f + (1 - \phi) / K_s \right]^{-1}, \tag{3}$$

where ϕ is a porosity, K_f is the bulk modulus of the fluid, $K_s \gg K_f$ is the effective bulk modulus of the solid (reinforcement) phase, and K is the drained bulk modulus of the frame determined by the relationship [35]

$$1 / K = 1 / K_s + \phi / K_\phi. \tag{4}$$

In Equation (4) $K_\phi \ll K_f$ is the pore volume bulk modulus. The components of the Biot effective stress tensor $\alpha = [\alpha_x \ \alpha_x \ \alpha_z \ 0 \ 0 \ 0]^T$ in a case of transversely isotropic material are defined as [35]

$$\alpha_x = 1 - (M_{xx} + M_{xy} + M_{xz}) / 3K_s; \alpha_z = 1 - (2M_{xz} + M_{zz}) / 3K_s. \tag{5}$$

The mobility tensor κ in Equation (2) is the ratio of the permeability tensor Ξ of a porous medium to the dynamic viscosity of the fluid μ_f :

$$\kappa = \Xi / \mu_f, \tag{6}$$

and the permeability tensor Ξ is related to the porosity by the Kozeny–Karman relation

$$\Xi = \Xi_0 \cdot \phi^3 / (1 - \phi^2), \tag{7}$$

where the symmetric tensor Ξ_0 is expressed in the form of a diagonal matrix ($\Xi_{x0} \ \Xi_{x0} = \Xi_{y0} \ \Xi_{z0}$) containing the components, which values usually obtained experimentally.

The significant computational complexity of solving the problem (1), (2), revealed in preliminary numerical experiments, made it important to simplify the mechanical part of the problem, i.e., refusal to use the system (1). This became possible due to the introduced assumptions described above. They allowed to introduce the effective compressive stress p_c , which depends on the applied external stress p_{appl} and pore pressure p_m according to

$$p_c = p_{appl} - \alpha_z \cdot p_m, \tag{8}$$

and to express the dependence of the fiber volume fraction $V_f = 1 - \phi$ on the compressive pressure, using the experimental data on the compressibility of the wet preform, borrowed in [36]. Approximations by 3rd order splines of this dependence and the corresponding dependence of Young’s modulus in the normal direction to the compressible surface on the fiber volume fraction are shown in Figure 1a,b.

In-plane Young’s modulus Y_x is taken to be n times ($n = 4$) greater than the modulus $Y_z(V_f)$. Taking into account the assumptions made, the bulk modulus of the compressible preform’s elastic frame can be expressed through Y_z modulus and ν_{zx} Poisson’s ratio

$$K_\phi = Y_z / (1 - 2\nu_{zx}). \tag{9}$$

Relation (8), together with the semi-empirical dependence $Y_z(V_f)$, makes it possible, by virtue of the assumptions made, to express the out-of-plane e_z and in-plane e_x strains of the preform in the form

$$e_z = (\phi - \phi_{max}^0) / (1 - \phi), \quad e_x = -\nu_{xz} \cdot e_z, \tag{10}$$

where ϕ_{max}^0 is the initial local porosity before resin infusion.

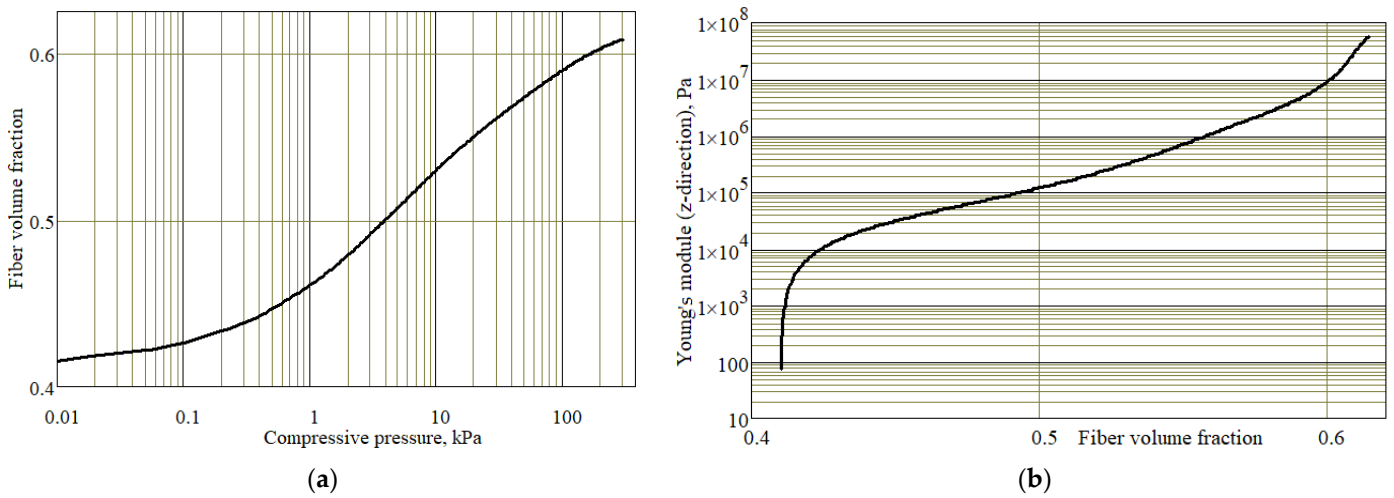


Figure 1. Compressive properties of the modeled wet preform: (a) Dependence of the fiber volume fraction on the compressive pressure; (b) Dependence of the Young’s modulus in z-direction on the fiber volume fraction.

The set of relations (2)–(10), from which system (1) is excluded, completes the formulation of the problem. The properties of the materials used in the model are presented in Table 1.

Table 1. Properties of the modeled system components.

Designation	Value	Meaning
$\nu_{xz}/\nu_{zx}/\nu_{xy}$	0.15/0.0375/0.3	Poisson’s ratios
Ξ_0	$(2.2 \cdot 0.5) \cdot 10^{-11} \text{ m}^2$	Minimum preform permeability components
Y_s	$5 \cdot 10^{10} \text{ Pa}$	Young’s modulus of reinforcing fibers
ν_s	0.3	Poisson’s ratio of reinforcing fibers
K_s	$4.17 \cdot 10^{10} \text{ Pa}$	Bulk modulus of reinforcing fibers
K_f	$2 \cdot 10^9 \text{ Pa}$	Bulk modulus of liquid resin
ρ_f	1200 kg/m^3	Mass density of liquid resin

3. Finite-Element Implementation of the Problem of Post-Infusion Pressure Application to Preform. Stand-Alone Version

3.1. Geometry and Finite-Element Meshing

To facilitate understanding of the ongoing processes, the geometry of the model is significantly simplified compared to real composite structures made using vacuum infusion technology, but the dimensions, although larger than those in experimental works [13,15,25,26], are commensurate with the composite structures of interest. The sizing decision was a compromise based on the viscosity of the resin to be used and the process duration. The appearance and dimensions of the preform are shown in Figure 2. The locations of the vacuum vent and resin are similar to those given in our works [33,34]. The distances d_{inl} and d_{out} from an arbitrary point in the preform to the resin gate and vacuum vent, respectively, which used when forming the initial conditions of the problem, are calculated by the formulas

$$d_{inl} = \sqrt{(x - x_{inl})^2 + (y - y_{inl})^2}, \quad d_{out} = \sqrt{(x - x_{out})^2 + y^2}, \quad (11)$$

where $x_{inl}, y_{inl}, x_{out}$ are the coordinates of the centers of the named ports.

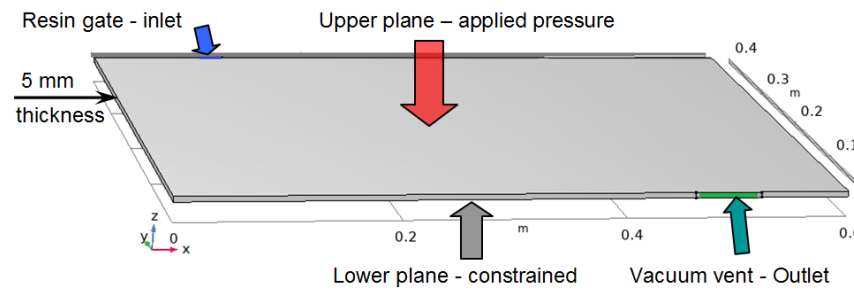


Figure 2. Geometry of the modeled system.

The size of the finite elements corresponded to the propagation velocity of the liquid resin. Preliminary numerical experiments with various FE mesh partitions determined the maximum value of the superficial fluid velocity, which reached 0.1 mm/s at the increasing external compressive pressure. Based on this result, the following final parameters of the FE meshing were adopted. A 2D mesh of triangular elements with sides 2 to 2.5 mm long with equal scale along the x and y axes, built on the upper surface of the preform and containing 38,016 elements, was extruded in three layers 1.66-mm thick in the direction of the lower surface. The resulting mesh, consisting of 76,464 triangular and rectangular boundary elements and 114,048 3D hexahedral elements, is shown in Figure 3. Modeling of all considered cases showed stable convergence of the computation.

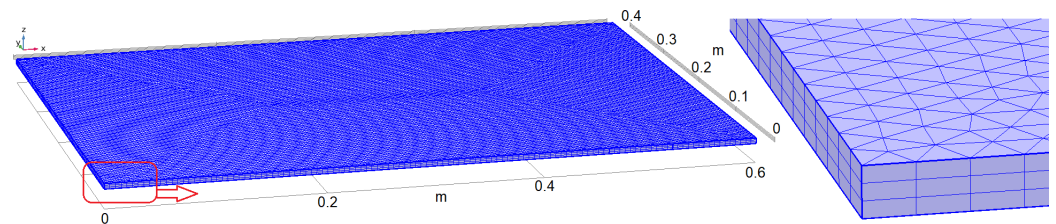


Figure 3. FE meshing of the preform volume.

3.2. Initial Conditions

Due to the fact that the start of the post-infusion simulation should occur after the completion of filling the preform with resin, the initial conditions for the pore pressure p_m , porosity ϕ , and viscosity μ of the resin should correspond to this time instant. However, the work of the described modeling tool is presented here in stand-alone mode. Therefore, before the start of the process, a preliminary stage is carried out, during which an arbitrarily given initial distribution of pore pressure p_m^{init}

$$p_m^{init}(x, y) = p_m^0(d_{inl}(x, y) / d_{max}) \tag{12}$$

is settled by solving the Darcy’s flow equation. The plot of the tabulated function p_m^0 is shown in Figure 4a, and the maximum distance to the inlet d_{max} for the considered geometry is taken to be 0.64 m. The simulation of the post-infusion stage began after the stabilization of the flow, when the mass flows of the liquid passing through the inlet and outlet, which initially had significantly different values, became almost equal, asymptotically approaching each other (see Figure 4b).

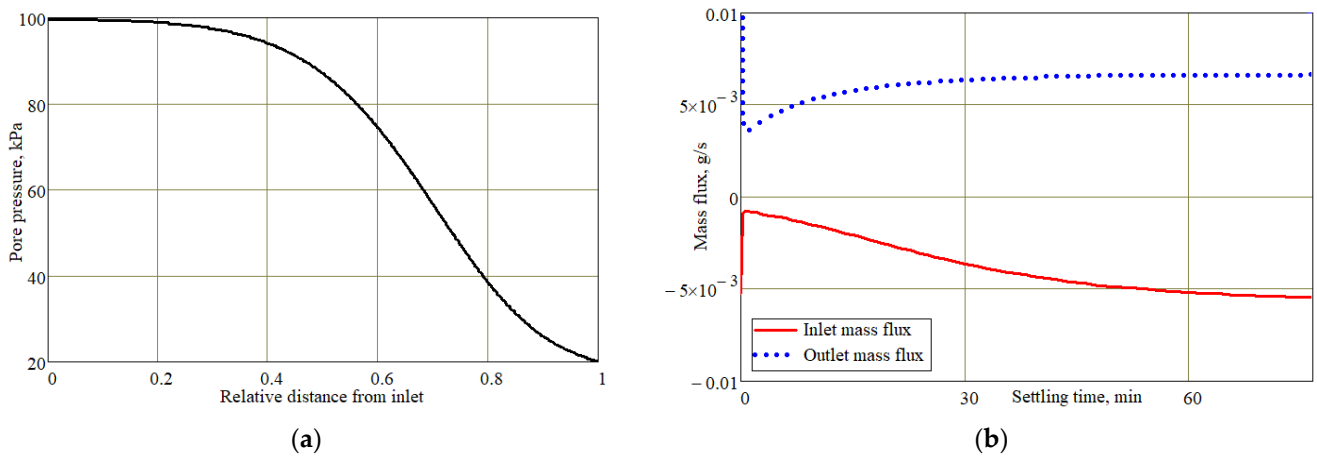


Figure 4. To the definition of the initial condition for pore pressure in the preform (explanation in text): **(a)** The plot of the auxiliary function p_{mi}^0 ; **(b)** Determination of the end point of resin flow stabilization (Mass flows have different signs because they are differently oriented with respect to the normal vectors of inlet and outlet).

The boundary conditions for inlet pressure $p_{inl} = 100$ kPa and outlet pressure $p_{out} = 20$ kPa, the values of which are accepted in most works studying the vacuum infusion of composites, are maintained unchanged throughout the duration of stabilization process. The results of pore pressure and fluid flow preliminary stabilization are shown in Figure 5.

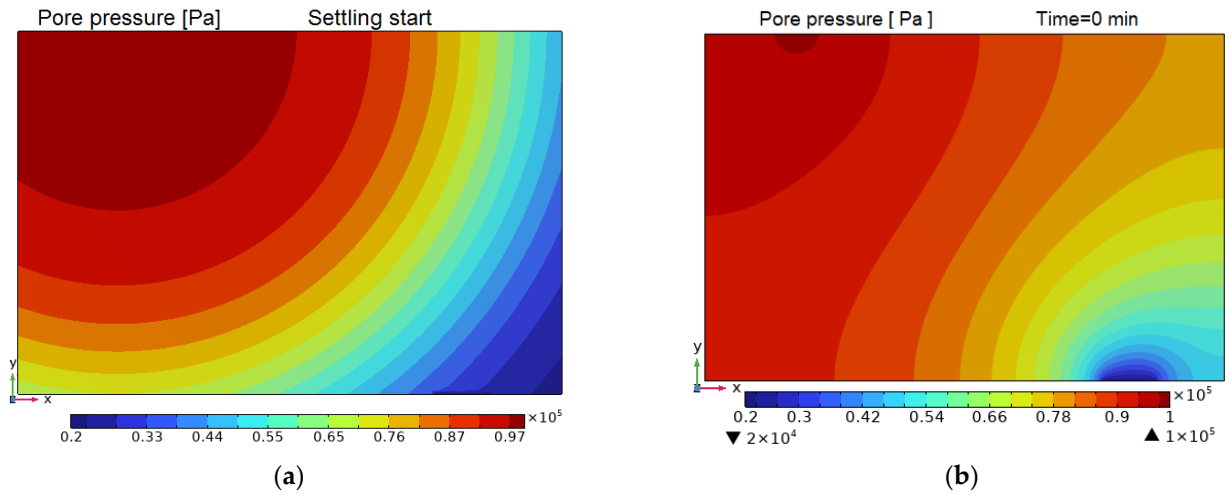


Figure 5. Initial **(a)** and steady state **(b)** pore pressure distributions in the preform before post-infusion exposure to controlled external pressure.

In the presented version of the process, no temperature or thermal-kinetic effects are taken into account. Therefore, the distribution of resin viscosity in the preform body is taken unchanged, approximately corresponding to the real distribution after 1.5 h, during which the resin filled the preform:

$$\mu(x, y) = 0.5 \cdot \left[0.1 + \tanh^2(d_{inl}(x, y) / d_{max}) \right] \text{ Pa}\cdot\text{s}. \tag{13}$$

This distribution is shown in Figure 6.

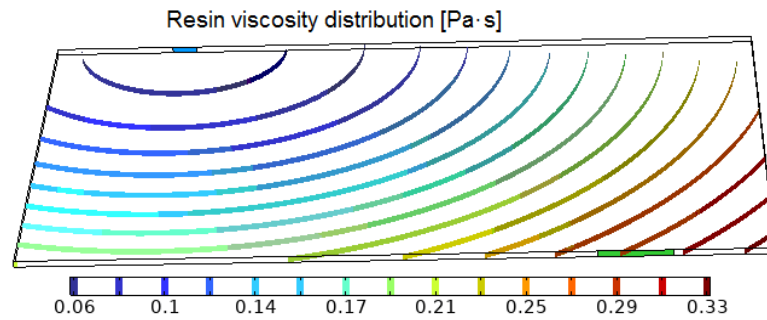


Figure 6. Spatial distribution of liquid resin viscosity.

3.3. The Darcy’s Law Equation and Boundary Conditions

The assumptions introduced in Section 2 reduced the problem to a single PDE (2). The complete problem statement was implemented in the Comsol Multiphysics environment, in the Multiphysics mode, which contains two main nodes: Darcy’s Law and Poroelasticity. Darcy’s law in the transient mode includes a sub-nodes Porous medium, where the diffusion equation has the form (14):

$$\rho_f S_p \frac{\partial p_m}{\partial t} + \nabla \cdot \rho_f [-\kappa(\nabla p_m)] = Q_m, \tag{14}$$

where the Darcy’s flow is accepted as the Flow model, and Storage model in the linearized form is a weighted sum of two compressibilities, of fluid $\chi_f = 1/K_f$ and of porous frame $\chi_p = 1/K$:

$$S_p = \phi \cdot \chi_f + (1 - \phi) \chi_p. \tag{15}$$

Mass source Q_m in Equation (14) is defined as

$$Q_m = -\rho_f \cdot (\alpha_z \cdot de_z / dt + 2 \cdot \alpha_x \cdot de_x / dt). \tag{16}$$

All boundaries except inlet and outlet are closed to fluid flow: $\mathbf{n} \cdot \mathbf{u} = 0$.

On the upper surface, at the moment of resin flow stabilization completion (hereinafter taken as zero time count), the external pressure gradually increases and then stabilizes according to the law

$$p_{appl}(t, \Delta t, p_{add}) = p_{atm} + p_{add} \cdot H_2(t, \Delta t), \tag{17}$$

where: H_2 is the Heaviside function with continuous second derivative, $p_{atm} = 100$ kPa—is the atmospheric pressure, p_{add} is an additional pressure, and Δt is duration of the pressure change (rise time). In all numerical experiments described below, $\Delta t = 10$ min is assumed, taking into account the inertance of the resin flow, depending on its viscosity and the permeability of the preform. Reducing this time was undesirable, since it could lead to a sharp change in flow velocities and numerical instability. This choice was also consistent with the specification of the Vacmobile 20/2 mobile vacuum system to be used.

This boundary condition is used unchanged in all simulated scenarios.

In the always open vacuum vent, the pressure $p_{vac} = 20$ kPa is initially maintained, which can remain unchanged during the entire post-infusion stage (no outlet control), or increase to atmospheric pressure p_{atm} with some delay t_{lag} after applying an external compressive pressure (outlet pressure control), as shown in Figure 7:

$$p_{out}(t, \Delta t, t_{lag}, p_{add}) = p_{vac} + (p_{atm} - p_{vac}) \cdot H_2(t - t_{lag}, \Delta t). \tag{18}$$

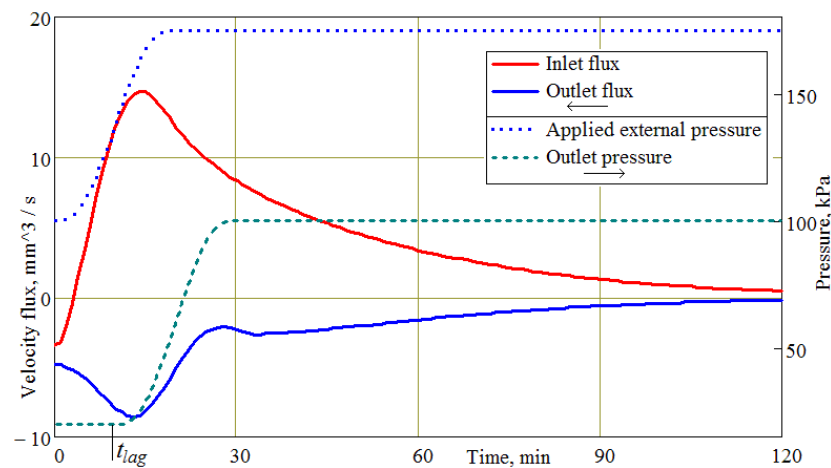


Figure 7. Combined time histories of fluid fluxes through the inlet and outlet since the beginning of the post-infusion stage and time dependencies in external compressive pressure and pressure in the vacuum vent.

The boundary condition for the resin gate is different for the two scenarios under study. In the first one, the inlet is open and the pressure in it is maintained equal to atmospheric $p_{int} = p_{atm}$, due to which resin flushing occurs. In the second scenario, at the stage of resin flow stabilization, the inlet is open, but after stabilization is completed, the inlet closes immediately: $\mathbf{n} \cdot \mathbf{u} = 0$. Therefore, Equation (14) is solved in two steps, each of which uses different boundary conditions for the resin gate.

The transient problem (14) with the initial and boundary conditions described above was solved using the BDF (backward differentiation formula) solver with automatic step determination, limited manually by values from 5 to 60 s at different stages of the process. The choice of these restrictions was performed at the preliminary setting of the computation parameters on the base of the actual process speed and the convergence plot analysis during simulation. To reliably ensure numerical stability, the value of restrictions per time step was assigned 3–5 times less than the steps offered by the BDF algorithm. At each time step, factorization and solving large systems of sparse equations were performed by the PARDISO direct solver, which is high performance, robust, memory efficient, and able to operate using both shared and distributed memory architectures.

3.4. Postprocessing of Calculation Results

The Comsol Multiphysics FE modeling tool allows you to reconstruct the spatial distribution in the simulated domain of any given variable and create a snapshot of that distribution at every time step. The probes of these variables defined in the software module (volume-averaged, maximum and minimum values) are used to plot their time dependences. Fluxes of velocity and transported fluid mass through the inlet/outlet surfaces are determined by calculating the corresponding surface integrals at each simulation step. Examples of simulation results presentation are given below.

4. Modeling Results

Figures 8–10 give a general understanding of the nature of changes after the application of controlled compression pressure in the distributions of the pore pressure, porosity, and thickness of the infused preform.

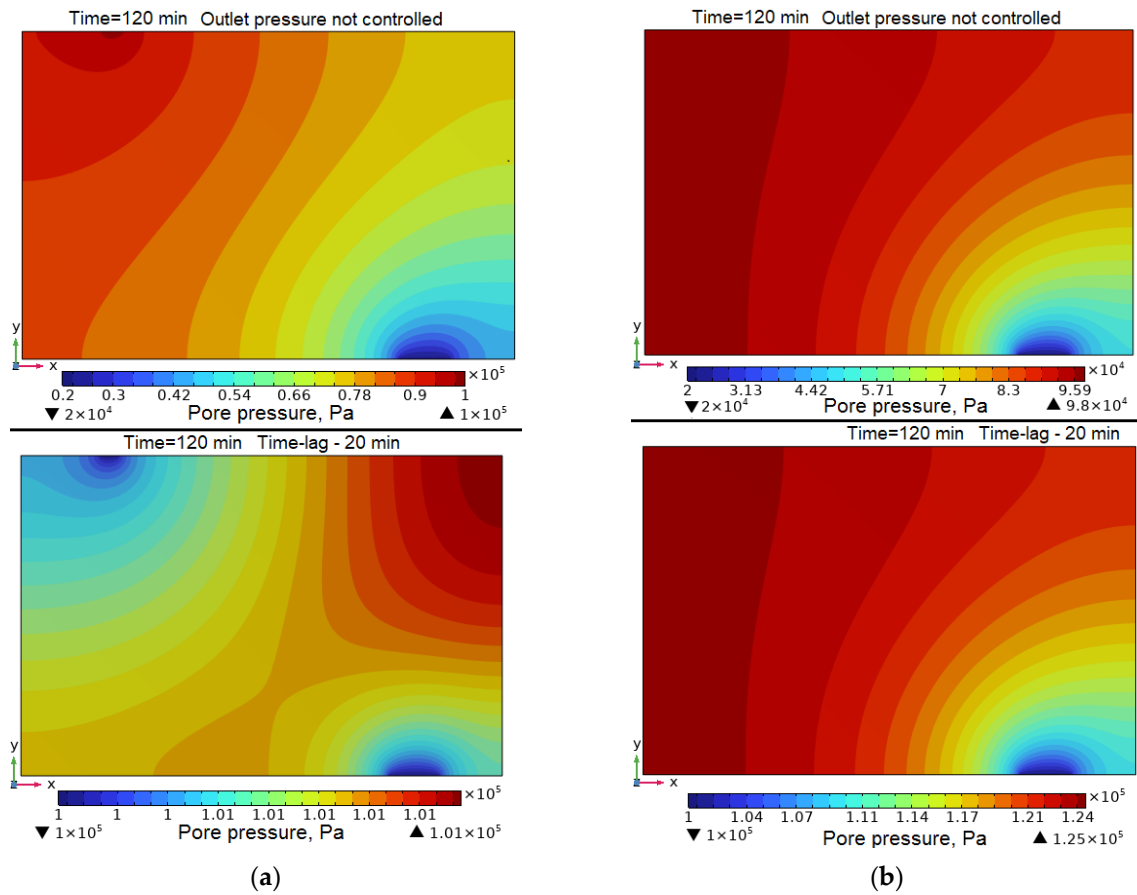


Figure 8. Distribution of pore pressure in preforms after 2 h of exposure to compressive pressure p_{appl} according to the 1st (a) and 2nd (b) scenarios. The upper pictures correspond to the case of a constant pressure at the outlet $p_{out} = p_{vac} = 20$ kPa, whereas the lower pictures correspond to the outlet pressure that began to grow 20 min after the start of the process and reached atmospheric $p_{out} = p_{atm} = 100$ kPa.

Figures 8–10 demonstrate significantly better post-processing results for the 1st scenario in terms of achieving a uniform distribution of pore pressure and preform wall thickness. In addition, outlet pressure equalization to atmospheric also improves the uniformity of the preform thickness distributions. Despite the fact that differences in the properties of the components used have a significant effect on the results of measurements in experiments, it should be noted that the results presented and the experimental data published in [25,26] are in good agreement. Thus, increasing the outlet pressure seems to be very appropriate. This is quite acceptable taking into account the fact that at the final stage of molding the structure, the viscosity of the resin increases significantly. However, such a solution requires the obligatory exclusion of the reverse flow from the vacuum line into the preform. This issue will be discussed below.

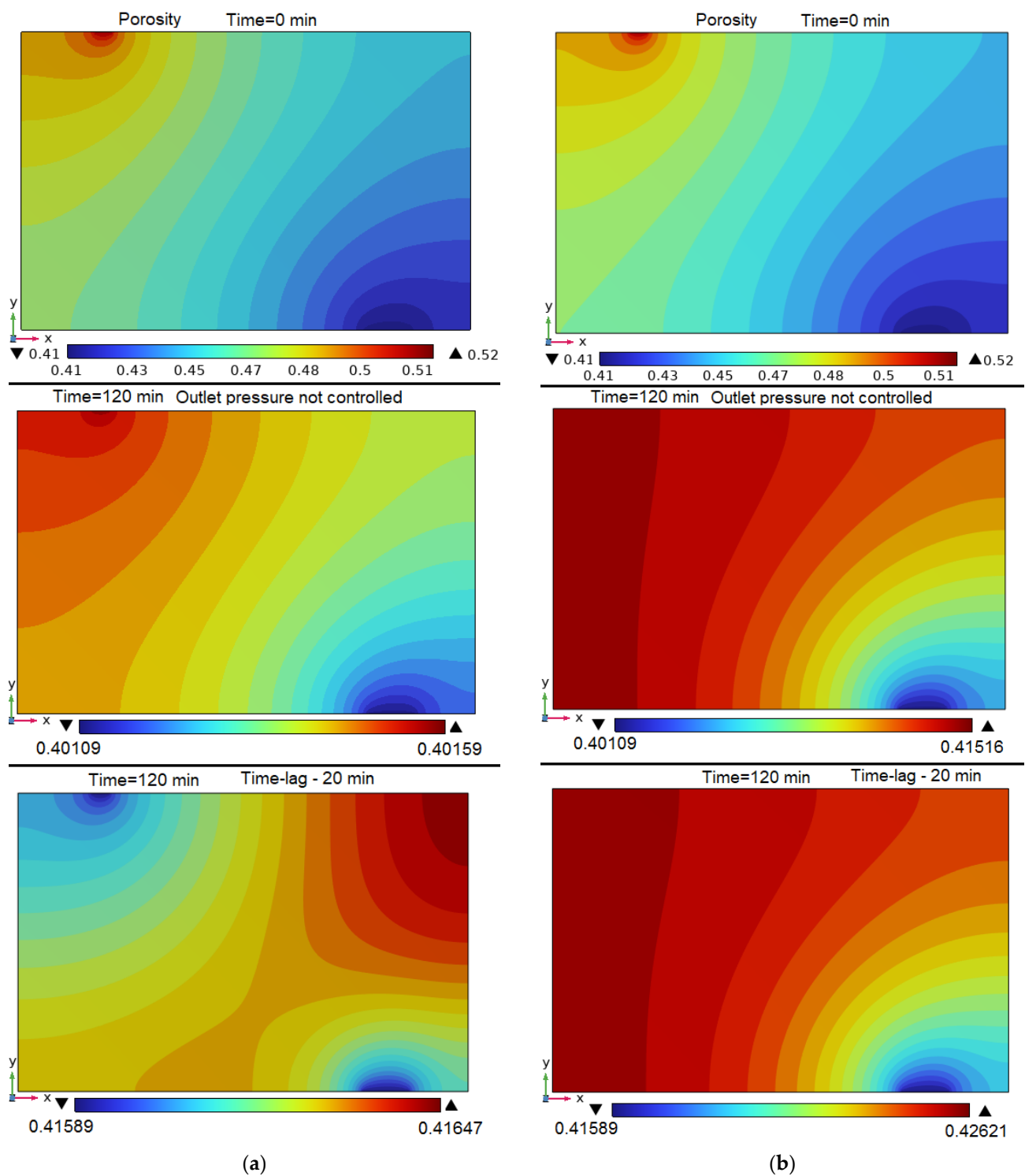


Figure 9. Distribution of preforms porosity at the start of the post-infusion compression (upper pictures) and after 2 h of exposure to compressive pressure p_{appl} according to the 1st (a) and 2nd (b) scenarios. The middle pictures correspond to the case of a constant pressure at the outlet $p_{out} = p_{vac} = 20$ kPa, whereas the lower pictures correspond to the outlet pressure that began to grow 20 min after the start of the external pressure growing and reached atmospheric $p_{out} = p_{atm} = 100$ kPa.

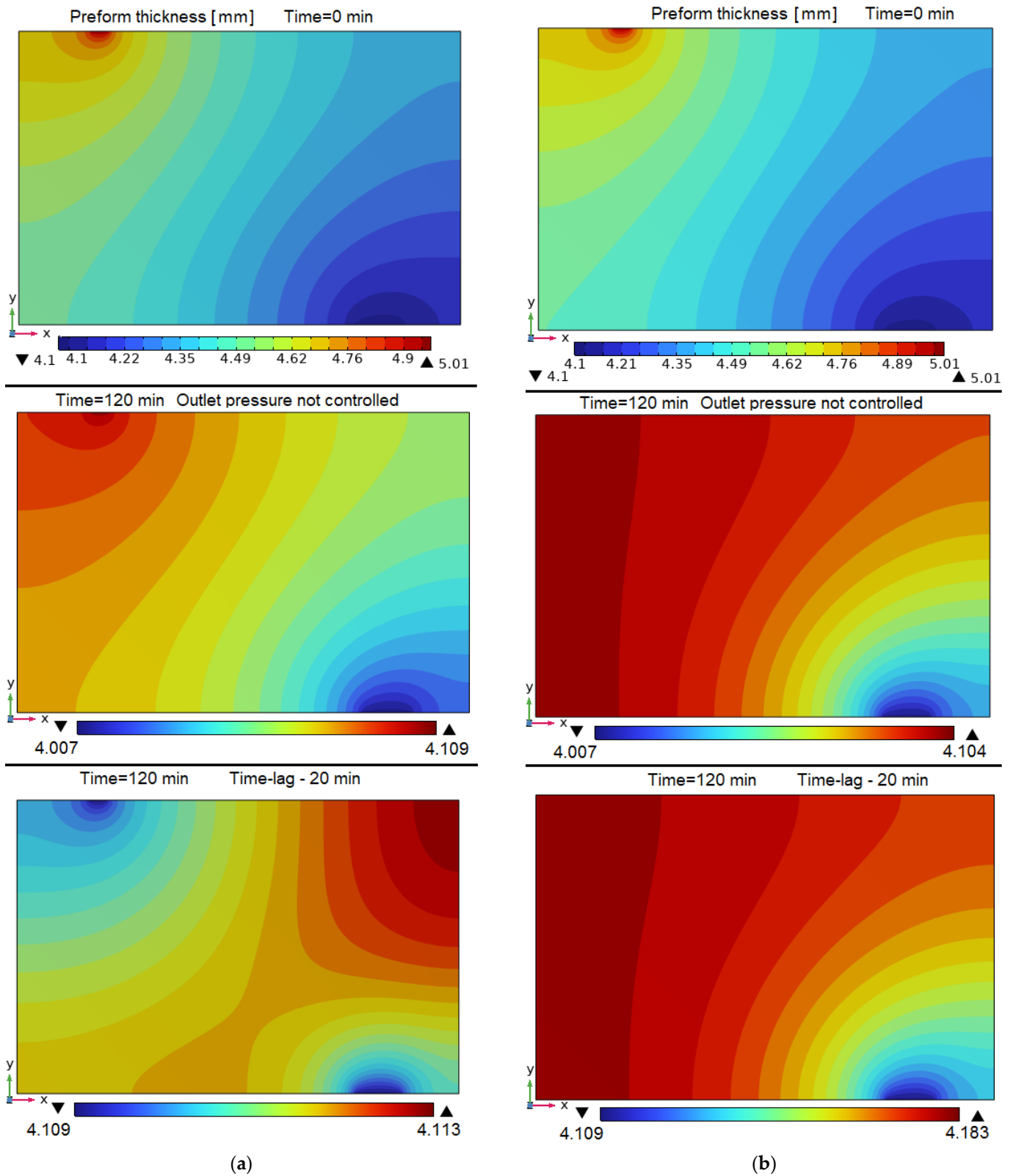


Figure 10. Distribution of preform thickness at the start of the post-infusion compression (upper pictures) and after 2 h of exposure to compressive pressure p_{appl} according to the 1st (a) and 2nd (b) scenarios. The middle pictures correspond to the case of a constant pressure at the outlet $p_{out} = p_{vac} = 20$ kPa, whereas the lower pictures correspond to the outlet pressure that began to grow 20 min after the start of the process and reached atmospheric $p_{out} = p_{atm} = 100$ kPa.

The influence of the layout and the mode of post-infusion pressures control on the dynamics of resin evacuation from the preform is demonstrated by the time dependences of the mass flow leaving through the inlet and outlet (see Figure 11).

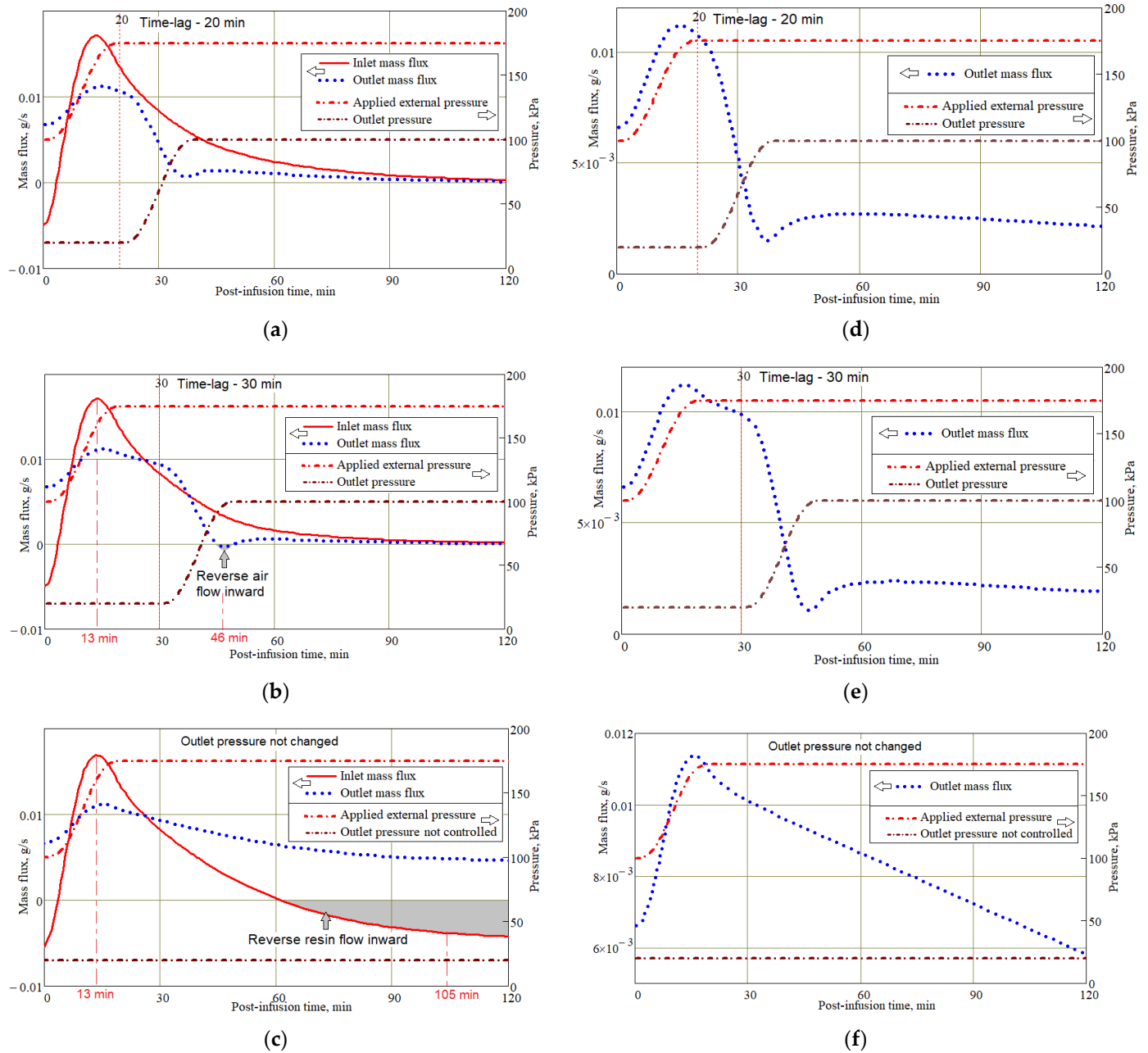


Figure 11. Time dependences of resin mass flows through the inlet and outlet for the first (a–c) and second (d–f) scenarios of post-infusion exposure, combined with graphs of changes in external compressive pressure and outlet pressure. Diagrams (a) and (d) correspond to the time-lag of the moment of pressure increase at the outlet of 20 min, (b) and (e)—30 min, a constant outlet pressure of 20 kPa—diagrams (c) and (f).

Attention should be paid to two extremely undesirable situations presented in Figure 11b,c. Figure 11b shows the reversal of the flow direction in the outlet. Namely, at the time of ~46 min, this flux is directed inside the preform. However, this means that the air contained in the resin trap will enter the preform. For comparison, the orientation of the streamlines at times 13 and 46 min is shown in Figure 12a,b.

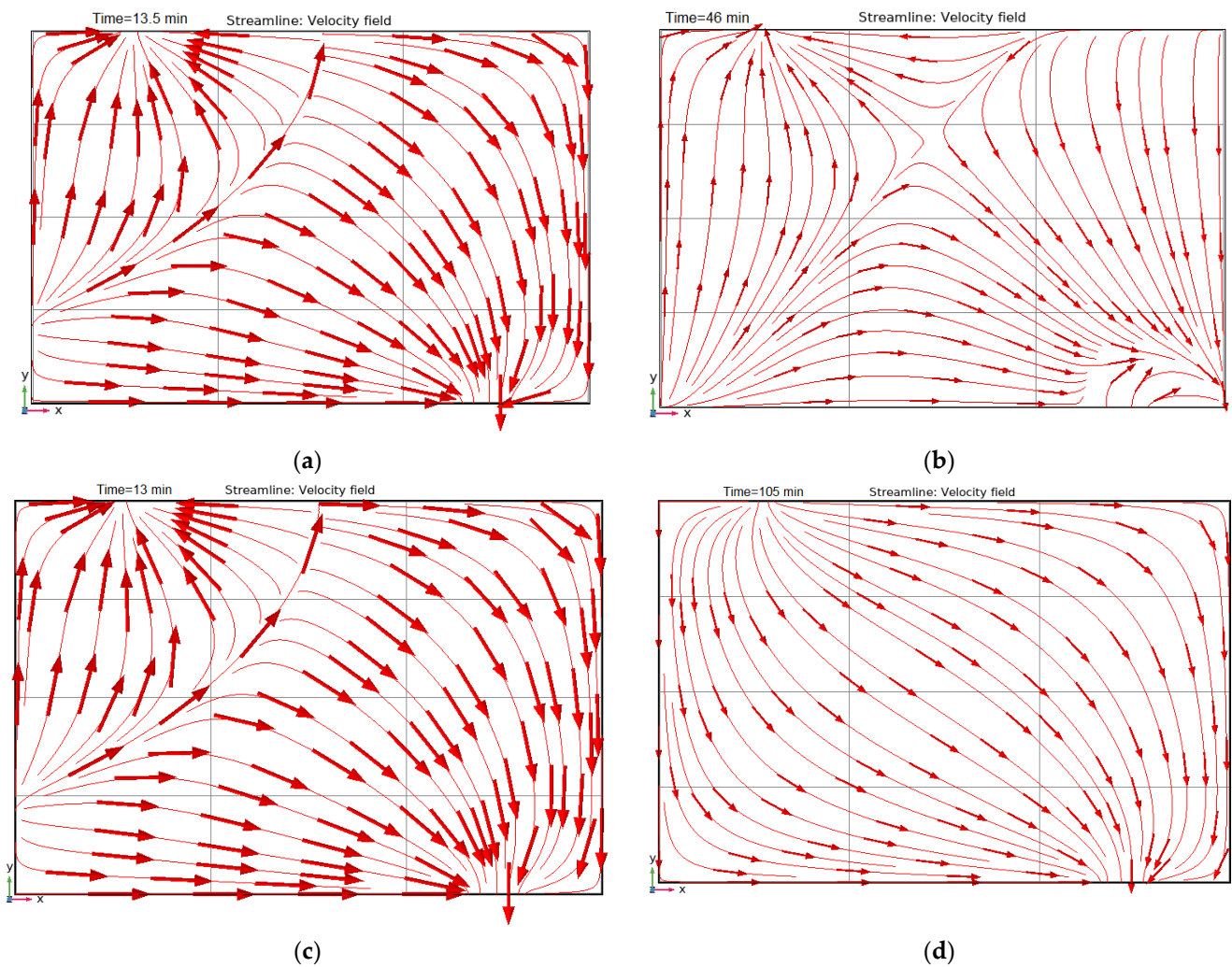


Figure 12. Maps of the resin streamlines in the preform under post-infusion application of external pressure according to the 1st scenario: (a,b) delay in the growth of the output pressure of 30 min; (c,d) without increase in outlet pressure (see Figure 11).

Figure 11c shows the situation when the excess resin that came out of the inlet returns inward to the preform. Such phenomena must also be excluded, especially when using highly active thermosetting resins. The distribution of streamlines at the times of 13 min and 105 min is shown in Figure 12c,d.

These considered critical situations demonstrate the importance of choosing the right delay time and outlet pressure growth rate when using the first scenario. Note that when modeling the second scenario, no such situations were found.

The groups of time dependences of the average pore pressure, its average gradient, and the accumulated volume of resin removed from the preform for various options for the post-infusion process implemented according to the first and second scenarios, presented in Figure 13, allow us to draw conclusions about the possibility of achieving the required quality indicators in the minimum time. Note that the diagrams in Figure 13a–d are built using the results of monitoring the corresponding probes throughout the entire duration of the process, while the diagrams in Figure 13e,f are obtained by integration of the time dependences of the mass fluxes of resin leaving the inlet and outlet of the type shown in Figure 11. It can be seen that the first scenario provides a much faster and better equalization of the pore pressure in the preform compared to the second scenario. The removal rate and total amount of excess resin removed is also significantly higher in the first case.

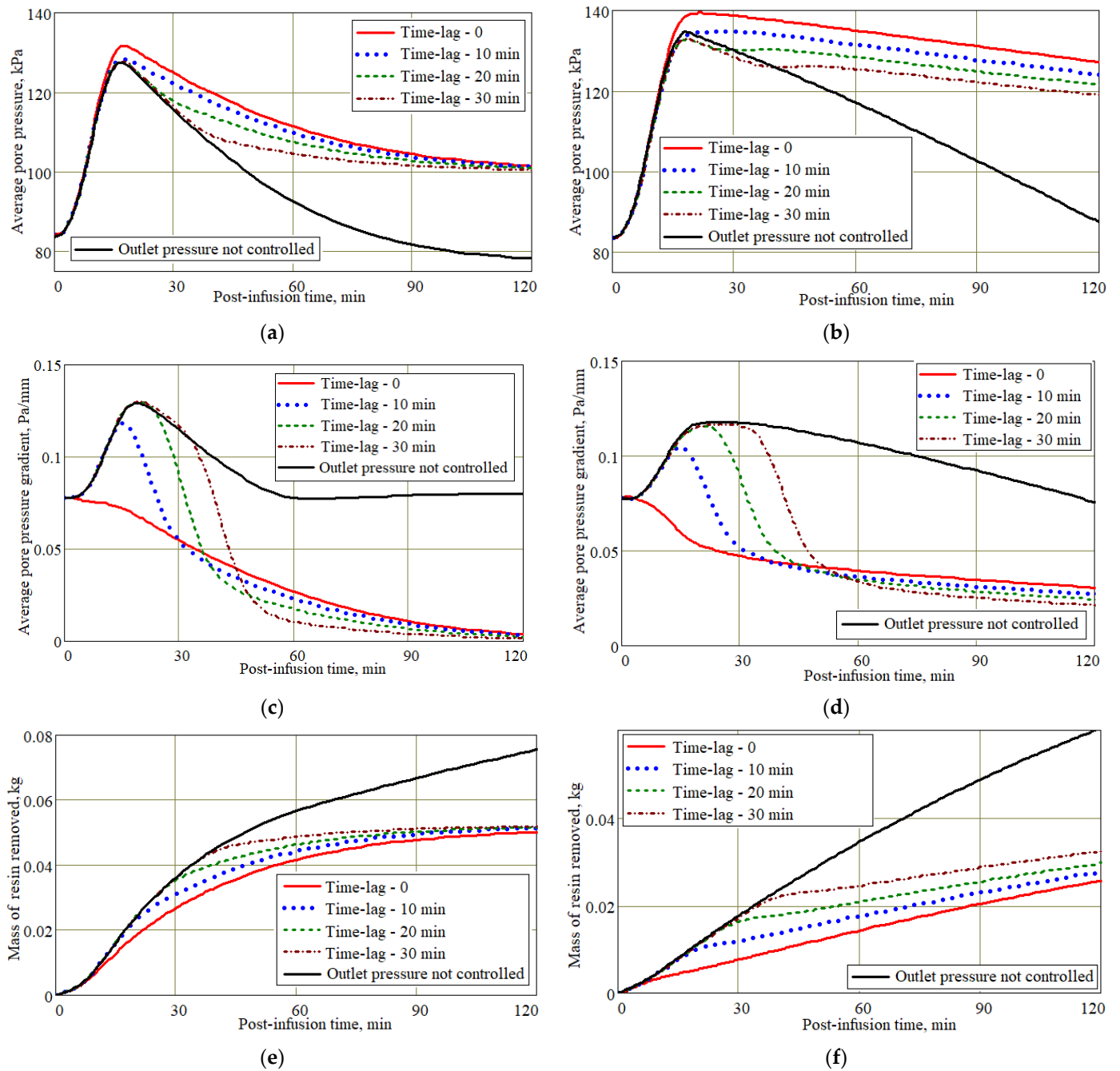


Figure 13. Time histories of average pore pressure (a,b), pore pressure gradient (c,d) and mass of resin removed (e,f) from the preform during the post-infusion stage realized using different the pressure control modes. The left plots (a,c,e) correspond to the 1st scenario, and the right ones (b,d,f) correspond to the 2nd scenario.

A comparison of the diagrams in Figure 13a,c,e shows that when implementing the first scenario, the use of a controlled increase in pressure at the outlet is preferable, since it provides a minimum pressure gradient in the preform and, consequently, more uniform porosity, although with a slightly smaller volume of removed excess resin than when maintaining vacuum pressure at the outlet. The dependence of the final indicators of the two considered process scenarios for various pressure control strategies is shown in Figure 14. Obviously, this information should be considered first when deciding on the choice of one or another method for improving the quality indicators of the composite structure obtained as a result of the vacuum infusion stage.

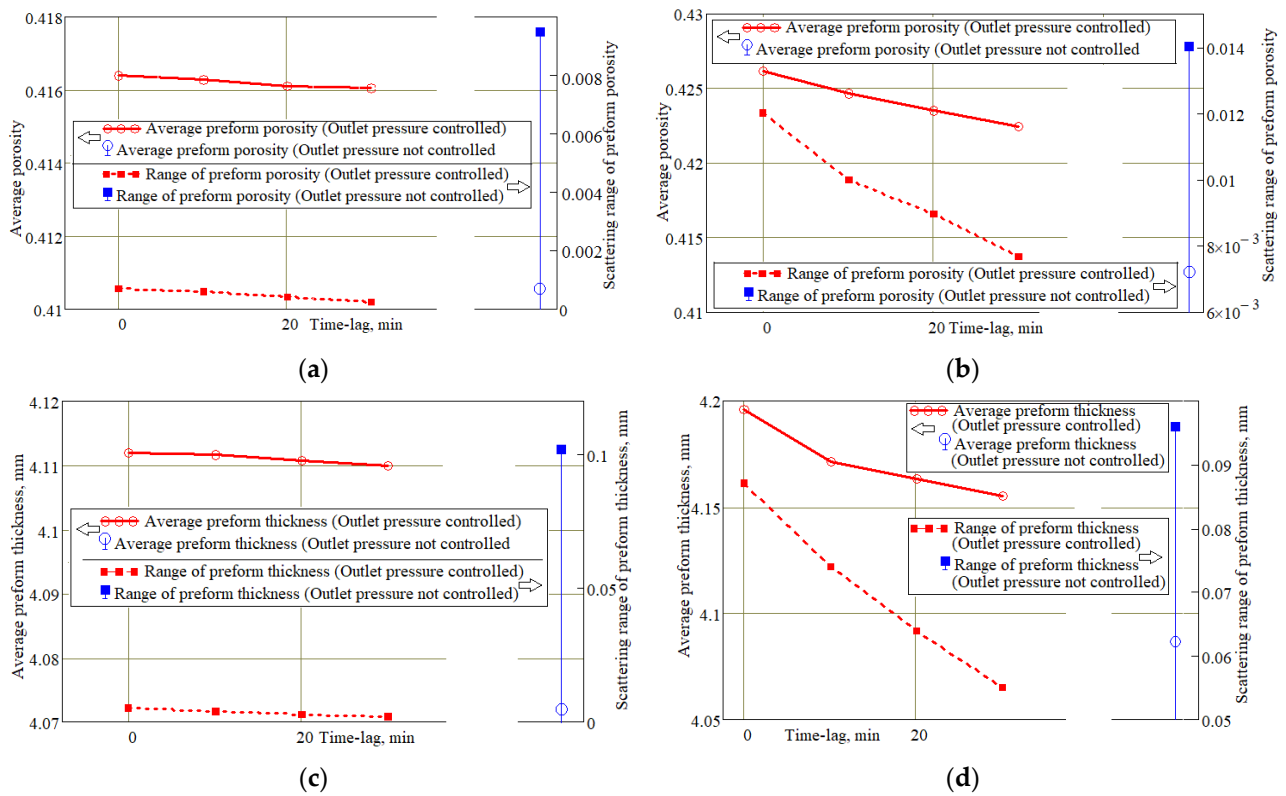


Figure 14. Comparative diagrams of the final indicators of porosity (a,b) and preform thickness (c,d) provided by the first (a,c) and second (b,d) scenarios of post-infusion exposure under various pressure control strategies.

5. Discussion

Even a cursory review of the results presented above shows that for the most part they qualitatively coincide with the experimental data published in [13–15,25,26]. This applies to completely matching conclusions about the most important results of the process formulated in [26], such as a decrease in the variation of the laminate thickness, the time of equalization of the pore pressure in the preform, and an increase in the fiber volume fraction by removing the excess resin. A comparison of the conclusions about the difference in the features of processes with an open and closed resin gate also demonstrates their identity. A detailed quantitative correspondence between the results presented in the article and the experimental results in [25,26] is not entirely justified due to possible differences and the lack of necessary information about the properties of the used preforms and resins, as well as due to the difference in the sizes of the experimentally studied (20 cm·15 cm) and modeled (60 cm·40 cm) preforms. Nevertheless, the analysis of process indicators, such as a decrease in preform thickness (experiment 15–25%, FE model ~20%), an increase in values, and a decrease in the variation in the fiber volume fraction (experiment 0.59–0.61, FE model ~0.59), confirms a good quantitative agreement between the results of both studies.

However, the results of the work of our FE model significantly exceed in terms of achievable quality indicators what is presented in the referred experimental works. There is no contradiction in this, since in the experiment there is always a significant element of uncertainty associated with the variation in the properties of components, regimes, with the occurrence of extraneous processes that are not taken into account in numerical models. The theoretical results presented in the article are physically correct, which is additionally confirmed by the equality of resin flows through both open ports after the flow in the preform is settled. A comparison of the instantaneous spatial distributions of pore pressure, porosity, and preform thickness demonstrates their significant similarity, which confirms their interdependence dictated by the governing equations.

With a consistently low pressure in the vacuum vent or with an uneven distribution of pore pressure, it is very important to make the right decision about the moment to stop the post-infusion process. The correct answer to this question depends on the actual rheological properties of the resin. The consequence of shutting down processes at low resin viscosity can be, for example, the continued not controlled equalization of the pore pressure in the preform, which can lead to deviations from the predicted parameters and specifications. Therefore, the first scenario with outlet pressure control seems to be more efficient, since it ensures equalization of the pore pressure, bringing it to atmospheric pressure, preventing spontaneous deformations of the preform. In some cases, to prevent the formation of areas with a sharply increased or decreased pore pressure, it is advisable to use several resin injection points, possibly with different throughputs, or runners. Then, the proposed modeling tool can also assist in the correct choice of a rational process layout.

Due to the introduced assumptions, the description of the processes taking place in the preform is greatly simplified. When the proposed tool is combined with the previously developed simulation module [33,34], which takes into account the thermal physics and kinetics of phenomena in resins, the picture of the reconstructed processes will be more realistic and complex. However, this inevitable complication, which makes it difficult to widely use vacuum infusion technologies in industrial practice, will make it possible to predict the results of ongoing processes with greater accuracy and, therefore, efficiency. However, a necessary condition for the successful operation of simulation systems similar to the one presented is the possibility of experimental determination of all the required properties of the components used.

Concerning more applied issues, it should be recognized that one of the most difficult problems in the technological support of vacuum infusion processes is the use of the required pressure chambers. A possible solution is to upgrade the autoclaves to include thermally insulated vacuum and resin lines with independent pressure control. This is a particular technical challenge, but process modeling for a preform of arbitrary geometry, filled at controlled temperature and external pressure, can be easily implemented after combining the previously developed [33,34] and considered software tools. The development of such a simulation tool, which will also optimize the cycle times, is the goal of our future research.

6. Conclusions

The aim of the presented study was to develop a software tool implemented as a FE model designed to simulate and optimize the post-infusion effect of controlled pressure on a preform that has passed the resin filling stage in order to homogenize the pore pressure as well as reduce and equalize the distribution of porosity, providing improved geometry and mechanical properties of the produced polymer-composite structure. The method used is based on poroelasticity equations with introduced assumptions, justified by the specific shape and boundary conditions for the molded structure. In the article, in relation to the simplified geometry of the simulated system, two scenarios for the implementation of post-infusion processes, which differ in the layouts and the control strategy, are considered. The results of the study made it possible to identify the main factors influencing the course of the simulated processes, critical situations, the consequence of which may be the occurrence of irreparable defects. A comparison of the simulation results with borrowed reliable experimental data confirmed the adequacy of the results and the acceptable computational complexity of the developed software tool. In conclusion, the possibility of using it with the previously developed FE module for modeling the infusion stage of the process in the practice of manufacturing polymer-composite structures with strict technical requirements is discussed.

Author Contributions: Conceptualization, S.S. and S.-H.C.; methodology, S.S.; software, I.Z.; validation, S.S. and N.S.; formal analysis, I.Z.; investigation, S.S. and I.Z.; resources, S.-H.C.; data curation, N.S.; writing—original draft preparation, S.S.; writing—review and editing, S.-H.C.; supervision, S.-H.C.; project administration, S.S.; funding acquisition, S.-H.C. All authors have read and agreed to the published version of the manuscript.

Funding: This research was funded by Ministry of Science and Technology of the Republic of China, grants number MOST108-2221-E-992-026-, MOST109-2221-E-992-091- (Taiwan R.O.C.) and by Russian Academy of Science, project 122020100339-7.

Acknowledgments: The authors are grateful for the valuable support of research aimed at developing new composite technologies to the leadership of the Institute of Polymer Engineering, The University of Applied Sciences Northwestern Switzerland FHNW.

Conflicts of Interest: The authors declare no conflict of interest.

References

- Heider, D.; Gillespie, J.W. VARTM variability and substantiation. *Jt. Adv. Mater. Struct. Cent. Excell.* **2008**. Available online: <https://pdfs.semanticscholar.org/3ddc/79c6cf459936fb8a069b27437c5596b220bd.pdf> (accessed on 20 October 2022).
- Cano, R.J.; Grimsley, B.W.; Jensen, B.J.; Kellen, C.B. High temperature VARTM with Larc polyimides. In Proceedings of the 36th International SAMPE Technical Conference, San Diego, CA, USA, 1 January 2004. 10p.
- Park, D.C.; Yu, T.; Park, S.J.; Shin, D.H.; Kim, Y.H. Improvement of impregnation quality on out-of-autoclave processed CFRP aircraft wing spar through resin flow simulation. *Funct. Compos. Struct.* **2021**, *3*, 025001. [\[CrossRef\]](#)
- Ekuase, O.A.; Anjum, N.; Eze, V.O.; Okoli, O.I. A Review on the Out-of-Autoclave Process for Composite Manufacturing. *J. Compos. Sci.* **2022**, *6*, 172. [\[CrossRef\]](#)
- Baker, A.; Dutton, S.; Kelly, D. *Composite Materials for Aircraft Structures*, 2nd ed.; AIAA: Blacksburg, VA, USA, 2004; 600p.
- El-Hajjar, R.; Tan, H.; Pillai, K.M. Advanced processing techniques for composite materials for structural applications. In *Developments in Fiber-Reinforced Polymer (FRP) Composites for Civil Engineering*; Uddin, N., Ed.; Woodhead Publishing: Oxford, UK; Philadelphia, PA, USA; New Delhi, India, 2013; pp. 54–78.
- Kar, K.K. *Composite Materials: Processing, Applications, Characterizations*; Springer: Berlin/Heidelberg, Germany, 2017; 690p.
- Almazán-Lázaro, J.A.; López-Alba, E.; Díaz-Garrido, F.A. The mechanical effect of monitoring and controlling the impregnation in the resin infusion process. *Polym. Compos.* **2022**, *43*, 1916–1926. [\[CrossRef\]](#)
- Matsuzaki, R.; Kobayashi, S.; Todoroki, A.; Mizutani, Y. Flow control by progressive forecasting using numerical simulation during vacuum-assisted resin transfer molding. *Compos. Part A Appl. Sci.* **2013**, *45*, 79–87. [\[CrossRef\]](#)
- Rubino, F.; Tucci, F.; Esperto, V.; Carlone, P. Filling Time Reduction in Liquid Composite Molding Processes. *J. Compos. Sci.* **2022**, *6*, 222. [\[CrossRef\]](#)
- Celle, P.; Drapier, S.; Bergheau, J.-M. Numerical modelling of liquid infusion into fibrous media undergoing compaction. *Eur. J. Mech. A-Solid* **2007**, *27*, 647–685. [\[CrossRef\]](#)
- Govignon, Q.; Bickerton, S.; Kelly, P.A. Simulation of the reinforcement compaction and resin flow during the complete resin infusion process. *Compos. Part A Appl. Sci. Manuf.* **2010**, *41*, 45–57. [\[CrossRef\]](#)
- Yalcinkaya, M.A.; Sozer, E.M. Effect of part thickness variation on the mold filling time in vacuum infusion process. *J. Reinf. Plast. Compos.* **2014**, *33*, 2136–2150. [\[CrossRef\]](#)
- Arulappan, C.; Duraisamy, A.; Adhikari, D.; Gururaja, S. Investigations on pressure and thickness profiles in carbon fiber-reinforced polymers during vacuum assisted resin transfer molding. *J. Reinf. Plast. Compos.* **2015**, *34*, 3–18. [\[CrossRef\]](#)
- Caglar, B.; Yenilmez, B.; Murat Sozer, E. Modeling of post-filling stage in vacuum infusion using compaction characterization. *J. Compos. Mater.* **2015**, *49*, 1947–1960. [\[CrossRef\]](#)
- Matveev, M.Y.; Belnoue, J.P.-H.; Nixon-Pearson, O.J.; Ivanov, D.S.; Long, A.C.; Hallett, S.R.; Jones, I.A. A numerical study of variability in the manufacturing process of thick composite parts. *Compos. Struct.* **2019**, *208*, 23–32. [\[CrossRef\]](#)
- Gajjar, T.; Shah, D.B.; Joshi, S.J.; Patel, K.M. Experimental study of thickness gradient and flow simulation in VARTM process. *Fibers Polym.* **2020**, *21*, 384–391. [\[CrossRef\]](#)
- Wu, D.; Larsson, R.; Blinzler, B. A preform deformation and resin flow coupled model including the cure kinetics and chemorheology for the VARTM process. *Int. J. Mater. Form.* **2021**, *14*, 421–434. [\[CrossRef\]](#)
- Ouezzan, A.; Mallil, E.H.; Echaabi, J. Manufacturing routes of vacuum assisted resin infusion: Numerical investigation. *J. Compos. Mater.* **2022**, *56*, 3221–3236. [\[CrossRef\]](#)
- Yu, Y.; Cui, X.; Liang, Z.; Qing, X.; Yan, W. Monitoring of three-dimensional resin flow front using hybrid piezoelectric-fiber sensor network in a liquid composite molding process. *Compos. Sci. Technol.* **2022**, *229*, 109712. [\[CrossRef\]](#)
- Jeong, J.M.; Eum, S.; On, S.Y.; Kageyama, K.; Murayama, H.; Uzawa, K.; Kim, S.S. In-situ resin flow monitoring in VaRTM process by using optical frequency domain reflectometry and long-gauge FBG sensors. *Compos. Struct.* **2022**, *282*, 115034. [\[CrossRef\]](#)
- Shin, J.H.; Anders, M.; Kim, D.; Jin, B.C.; Nutt, S. Effects of post-infusion dwell on vacuum infusion of thermoset composites toughened by thermoplastic interlaminar veils. *J. Compos. Mater.* **2021**, *55*, 1419–1433. [\[CrossRef\]](#)

23. Mostafa, N.H.; Ismarrubie, Z.N.; Sapuan, S.M.; Sultan, M.T.H. Fibre prestressed polymer-matrix composites: A review. *J. Compos. Mater.* **2017**, *51*, 39–66. [[CrossRef](#)]
24. Mohamed, M.; Selim, M.M.; Ning, H.; Pillay, S. Effect of fiber prestressing on mechanical properties of glass fiber epoxy composites manufactured by vacuum-assisted resin transfer molding. *J. Reinf. Plast. Compos.* **2020**, *39*, 21–30. [[CrossRef](#)]
25. Yalcinkaya, M.A.; Sozer, E.M.; Altan, M.C. Fabrication of high quality composite laminates by pressurized and heated-VARTM. *Compos. Part A Appl. Sci. Manuf.* **2017**, *102*, 336–346. [[CrossRef](#)]
26. Yalcinkaya, M.A.; Sozer, E.M.; Altan, M.C. Dynamic pressure control in VARTM: Rapid fabrication of laminates with high fiber volume fraction and improved dimensional uniformity. *Polym. Compos.* **2019**, *40*, 2482–2494. [[CrossRef](#)]
27. Shin, D.D.; Hahn, H.T. Compaction of thick composites: Simulation and experiment. *Polym. Compos.* **2004**, *25*, 49–59. [[CrossRef](#)]
28. Robinson, M.J.; Kosmatka, J.B. Analysis of the post-filling phase of the vacuum-assisted resin transfer molding process. *J. Compos. Mater.* **2014**, *48*, 1547–1559. [[CrossRef](#)]
29. Shah, D.U.; Clifford, M.J. Compaction, permeability and flow simulation for liquid Composite moulding of natural fibre composites. In *Manufacturing of Natural Fibre Reinforced Polymer Composites*; Salit, M.S., Jawaid, M., Yuso, N.B., Hoque, M.E., Eds.; Springer: London, UK, 2015; pp. 65–100.
30. Young, W.B. Three-dimensional modeling of the filling process in VARTM including the fiber compaction effect. *Int. J. Adv. Eng. Tech.* **2016**, *50*, 122–127.
31. Sorrentino, L.; Bellini, C.; Gerevini, E. New methodology to determine the compressibility curve in a RIFT process. *J. Compos. Mater.* **2014**, *48*, 1233–1240. [[CrossRef](#)]
32. Yenilmez, B.; Sozer, E.M. Compaction of e-glass fabric preforms in the vacuum infusion process: (a) use of characterization database in a model and (b) experiments. *J. Compos. Mater.* **2013**, *47*, 1959–1975. [[CrossRef](#)]
33. Shevtsov, S.; Zhilyaev, I.; Chang, S.-H.; Wu, J.-I.; Snezhina, N.; Huang, J.-Y. Two-stage numerical approach for reliable recognition of dry spots at the VAP infusion of large composite parts of complex shape. *Compos. Struct.* **2021**, *259*, 113437. [[CrossRef](#)]
34. Shevtsov, S.; Zhilyaev, I.; Chang, S.-H.; Wu, J.-K.; Snezhina, N. Multi-Criteria Decision Approach to Design a Vacuum Infusion Process Layout Providing the Polymeric Composite Part Quality. *Polymers* **2022**, *14*, 313. [[CrossRef](#)]
35. Cheng, A.H.D. *Poroelasticity. Theory and Applications of Transport in Porous Media*; Springer International Publishing: Cham, Switzerland, 2016; Volume 27, 893p.
36. Grimsley, B.W.; Hubert, P.; Song, X.-L.; Cano, R.J.; Loos, A.C.; Pipes, R.B. *Flow and Compaction during the Vacuum Assisted Resin Transfer Molding Process*; NASA Tech Report; NASA Langley Research Center: Hampton, VA, USA, 2001; 15p.